Structural Modification and Performance Enhancement of Zirconium Oxide with Copper Doping for Photo Catalytic and Antibacterial Applications

Suresh Kumar J.[1,2], Shyamala P.[1]*, Gouthamsri S.[2] and Ramanaiah M.[2]*
1. Department of Chemistry, Andhra University, Visakhapatnam-530003, INDIA
2. Department of Chemistry, Aditya Institute of Technology and Management, Tekkali-532201, INDIA
*shyamalapulipaka06@gmail.com; ramanaiahmalla4@gmail.com

Abstract
Zirconium oxide (ZrO_2) and copper-doped zirconium oxide (Cu-ZrO_2) nanoparticles (NPs) were synthesized via a sol-gel combustion method to study the influence of doping on their photocatalytic and antimicrobial properties. X-ray diffraction (XRD) analysis confirmed a mixed tetragonal and monoclinic phase structure with decreasing crystallite size at higher dopant concentrations. The NPs were characterized using FTIR, XRD, SEM-EDX, XPS and UV-Vis spectroscopy. SEM revealed spherical morphology with minimal agglomeration. Under visible light, Cu-ZrO_2 NPs exhibited enhanced photo- catalytic activity, degrading 96% of malachite green (MG) dye within 120 min. Antimicrobial assays demonstrated superior activity of Cu-ZrO_2 against S.aureus, with an inhibition zone of 8 mm compared to E.coli.

Keywords: Sol-gel, Cu-doped Zirconium oxide, Photo-catalysis, Antibacterial activity.

Introduction

The discharges of industrial wastewater, particularly wastewater from industrial textile industries, into the aquatic environment have been associated with severe environmental and health problems due to various non-biodegradable dyes and biological contaminants[8]. Synthetic dyes like malachite green (MG) are cationic triphenylmethane dyes highly persistent and carcinogenic hazardous chemicals often used in the dyeing operation[6]. As a result of the shortcomings in terms of high cost, high energy consumption and toxic secondary waste generation associated with conventional dye removal approaches, researchers have focused on providing lasting solutions to industrial wastewater treatment based on the complement of the conventional methods with highly efficient and sustainable water treatment methods[34].

Advanced oxidation processes involving the generation of highly chemical oxidants have shown effective degradation of a wide range of organic contaminants in polluted water[31]. Advanced oxidation processes such as heterogeneous photocatalysis, can be achieved by combining a titania-based catalyst with UV–visible light and it is more effective in decomposing recalcitrant complex organic pollutants than conventional methods[31]. Nanotechnology and nanomaterials have the capability to secure sustainability in the field of industrial wastewater treatment providing inventive technologies due to their ability to control the materials' functions and properties to be adequate with specific demand[10]. Various techniques based on nanotechnology were reported in the literature for wastewater remediation, which may be broadly classified into four major categories including biological, chemical, physico-chemical and physical methods[28]. Most of these techniques are suffering from the main two limitations, which are the required remediation time for process completion and the sludge disposal after finishing the remediation process.

Photo-catalytic degradation is a well-accepted favorable technique with great efficiency to completely degrade any organic compounds in the contaminated wastewater to convert them into harmless final products to human beings and the environment using a proper photocatalyst in presence of light radiation by producing highly reactive hydroxyl (OH•) radicals, which can convert water pollutants into relatively unharmful end products like CO_2, H_2O and other inorganic ions[14].

Photo-catalytic technology has the ability to address the first problem concerned with remediation time with tangible solutions for the remediation of dyes from industrial effluents. However, this technology still suffers from the problem of sludge disposal after the process completion. Thus, it is ethically imperative to address the issue to provide a congenial solution for the disposal of sludge to guarantee the sustainability of photocatalytic technology[15]. One of the alternatives is to use eco-friendly compatible photocatalytic materials, which will have less impact on the environment and ecology. A key parameter governing the performance of the photocatalytic materials is the generation of continuous electron reflux for producing highly reactive hydroxyl (OH•) radicals responsible for dyes degradation at industrial effluents.

Many oxide and sulfide materials such as ZnO, SiO_2, SnO_2, CeO_2, ZrO_2, CuO, MnO_2, TiO_2 and ZnS, CdS and Cu_2S[12] are widely used in the process of photocatalysis. In particular, ZrO_2 is considered an important material for use in photocatalysis because of its low-cost, non-toxic and eco-friendly features. ZrO_2 is a well-established ceramic material where the physical and chemical properties depend strongly on the structural phase leading to a variety of applications. There are many reports that describe the potential applications in thermal barrier coatings, refractory materials,

oxygen sensors, bioceramics, catalysis and electrolyte gate dielectrics[3].

Zirconium oxide is a wide bandgap (5.0–5.5 eV) semiconductor material that can be applied for catalytic purposes under both UV and visible irradiation[12]. It has good thermal, mechanical, electrical and optical properties such as low thermal conductivity, high hardness, high fracture toughness, high refractive index, optical transparency and high corrosion resistance and polymorphic nature.

The energy gap in pristine ZrO_2 can be reduced via combination with a variety of metal ions such as Ce, Mn, Cu, Mg, Fe, Ni, Co and Zn[26]. The doping of metal ions can be induced defect into ZrO_2 matrix. It is mostly related with changing in crystalline size, shape, as well as the decreasing energy gap. The modified ZrO_2 nanoparticle produced high photo catalytic efficiency. Among these, copper (Cu) is an important material that can be used for doping because of its high electronic conductivity, low expense and considerable avail ability[1]. Copper is generally found as Cu^{2+} in its ionic state and has an ionic radius (0.72 Å) which is similar to that of zirconium (Zr^{4+}) (0.80 Å). Cu ions can be doped easily into the ZrO_2 host lattice. It is well known that Cu^{2+} ions are incorporated into ZrO_2 to induce the formation of a host lattice via oxygen vacancies, decreasing the energy gap of ZrO_2 improving the optical, electrical and photocatalytic proper ties of ZrO_2.

Several techniques have been adopted for the synthesis of ZrO_2 nanoparticles including sol–gel techniques, spray pyrolysis, precipitation techniques, the combustion method and hydrothermal processes[17]. Among various synthesis methods, sol-gel combustion offers a simple, cost-effective and scalable approach to producing high-purity ZrO_2 nanoparticles with controlled size and morphology. According to the literature, most research has been carried out using Mn-doped ZrO_2, Fe-doped ZrO_2, Ni-doped ZrO_2 and Co-doped ZrO_2[2,16]. Even though a few studies have been carried out, structural, morphological, photoluminescence and photocatalytic investigations on Cu-doped ZrO_2 NPs are not sufficient. Nanostructured materials could also be used in biomedical applications. In this study, we have investigated the anti-bacterial activity of zirconia nanoparticles in addition to their photocatalytic activity. Many studies on metal oxide nanoparticles such as TiO_2, MgO, ZnO and ZrO_2 for anti-bacterial activity have been conducted[18].

In the present study, ZrO_2 and Cu-doped ZrO_2 nanoparticles were prepared by a solgel-combustion method. The products were analyzed by XRD, UV–Vis absorbances, FT-IR, SEM with EDS and XPS spectroscopy. Further, the Cu-doped ZrO_2 nanoparticles was used to study the photocatalytic activity using Malachite Green (MG) dye under visible light irradiation. The antibacterial activity of zirconium nanoparticles was also examined. The novelty of this work provides that the substitution of Cu in ZrO_2 shows the advantage to enhance the photocatalytic and anti-bacterial properties. There are very less reports on the photocatalytic and anti-bacterial properties for Cu-doped ZrO_2 nanoparticles; these special properties could be used for environmental cleanup, display devices and biomedical devices.

Material and Methods

Materials: The desirable solutions were prepared with help of double distilled water and all chemicals used in this synthesis are of analytical grade. Zirconium chloride ($ZrCl_4$), copper chloride ($CuCl_2$), nitric acid (HNO_3), ethylene glycol ($C_2H_6O_2$) and glycine ($C_2CH_5NO_2$) were procured from Merck Company, India. The bacteria such as *E.coli* (Gram –ve) and *S.aureus* (Gram +ve) are collected from IMT, Chandigarh.

Preparation of copper doped ZrO_2 NPs: To prepare a Cu-doped ZrO_2 NPs, the following steps were followed: In a 150 mL Pyrex glass beaker, 20 mL of $CuCl_2$, 20 mL of ethylene glycol and 3.2 mL of HNO_3 were mixed with glycine (fuel for combustion). The mixture was stirred for 15 minutes. In another beaker, the required amount of $ZrCl_4$ (based on weight percentage), 20 mL of 1,2-ethanediol and 3.5 mL of deionized water were combined for the hydrolysis process. solution I was then stirred vigorously while Solution II was slowly added drop-by-drop. This resulted in a colloidal suspension.

Aging and Drying: The suspension was stirred for additional 90 minutes and then stored for 48 hours. Finally, the product was thoroughly washed with water and oven-dried for 8 hours. A similar process was used to create undoped ZrO_2 and was stored in desiccators for further analysis.

Instrumentation: We synthesized Cu-doped ZrO_2 nanohybrids using a sol-gel - combustion method with glycine as fuel. We then characterized their optical, morphological and electrical properties using advanced analytical techniques. X-ray diffraction (XRD) analysis was performed using a Bruker AXS D8 diffractometer with Cu-Kα radiation and a scan rate of 0.02° per minute. Scanning electron microscopy (SEM) coupled with energy-dispersive X-ray spectroscopy (EDX) was conducted using a Shimadzu IR prestige 2 instrument with an FTIR range of 4000 to 500 cm^{-1}. X-ray photoelectron spectroscopy (XPS) analysis was performed with a PHI 5000 versa probe III.

Brunauer–Emmett–Teller (BET) analysis was performed using the BELSORP II Mini, a product of BEL MicrotracBEL Corp. Finally, the optical properties of the synthesized samples were investigated using a LabIndia UV-3092 UV-visible spectrophotometer operating in the wavelength range of 200-800 nm.

Malachite green dye degradation: We evaluated the photocatalytic activity of Cu-doped ZrO_2 nanohybrid and

undoped ZrO_2 for degrading malachite green (MG) dye, a common pollutant, under visible light irradiation. A photoreactor, designed based on established literature[12], was illuminated with a metal halide light source. To ensure a uniform mixture, the reaction solution containing the catalyst and MG dye was stirred using a magnetic stirrer for 30 minutes to achieve adsorption-desorption equilibrium. Subsequently, the solution was exposed to visible light until the MG dye degraded completely. We periodically collected aliquots of the solution to monitor the degradation rate using UV-Visible spectroscopy. The percentage of MG dye degraded by photocatalysis was calculated using the following equation 1:

$$\%\ MG\ degradation = \frac{A_o - A_t}{A_o} x\ 100 \quad (1)$$

where A_t and A_o represent the absorbance of the MG dye solution at time 't' and the initial time respectively.

Antimicrobial activity: Muller Hinton Agar Medium (High-Media) was dissolved in water in 500 mL conical flask and was sterilized in an autoclave at 121°C, 15lbs for 15 min and poured in sterilized Petri plates. The antibacterial activity of sample was evaluated by Agar Well Plate Method[24]. Inoculum was spread over the surface of agar plates with sterile cotton swab. To test the antibacterial activity, samples were dissolved in DMSO and some liquid samples were added directly with aliquots of the compound (500µl/mL, 200µl/mL, 100µl/mL) and then they were directly pipetted into the wells which were already inoculated with specific species i.e. Gram-ve (*E.coli*) and Gram+ve (*Staphylococcus*) and then plates were incubated for a period of 24 h at 37°C in an incubator and the diameter (mm) of the clear inhibitory zone formed around the discs was measured.

Results and Discussion

X-ray diffraction (XRD) analysis: Fig. 1 shows the XRD patterns of pure and copper-doped ZrO_2 NPs. The presence of sharp, well-defined peaks shows that the processed samples are extremely crystalline. Pristine ZrO_2 peaks were found at (2θ values) 29.58°, 30.46°, 35.4°, 39.06°, 50.48°, 59.96° related to the (111), (101), (110), (002), (112) and (121) reflectance planes suggesting the formation of the tetragonal ZrO_2 phase (JCPDS Card no. 88-1007). Cu doped ZrO_2 NPs are indicated by the high intense peaks at 31.84°, 34.46°, 36.24°, 38.92°, 47.62°, 56.66°, 62.9° and 67.92°, which correspond to the reflectance (011), (002), (110), (120), (212) (013) (202) and (132) planes and thus indicate the presence of the monoclinic ZrO_2 phase (JCPDS No. 81-1319).

From phase analysis, in Cu doped ZrO_2, it was noted that the Cu dissolved into the lattice of ZrO_2 with changes in the original phase. It shows the dopant led to an increase in shifting at 2θ values in the lift direction. This change is essentially owing to the variance in ionic radii of Cu^{2+} and Zr^{4+}, however, Cu^{2+} ions may also penetrate the host lattice via the substitution or interstitial mode, as previously reported[12].

The average crystallite sizes (S) of products were estimated using the Debye–Scherrer equation[29]:

$$S = \frac{k\lambda}{\beta cos\theta} \quad (2)$$

where the constant 'k' = 0.9, 'λ' is the wavelength of the radiation (Cu-Kα = 0.15405 nm), 'θ' is the diffraction angle and 'β' is the line width. The average crystallite sizes of the pristine ZrO_2 and Cu-doped ZrO_2 nanoparticles were calculated as 26.1 nm and 20.3 nm respectively.

Morphology and particle size: The effect of Cu doping on the morphology of ZrO_2 nanoparticles is investigated by Scanning electron microscope (SEM). The micrographs of undoped and copper-doped ZrO_2 nanoparticles are shown in fig. 2.

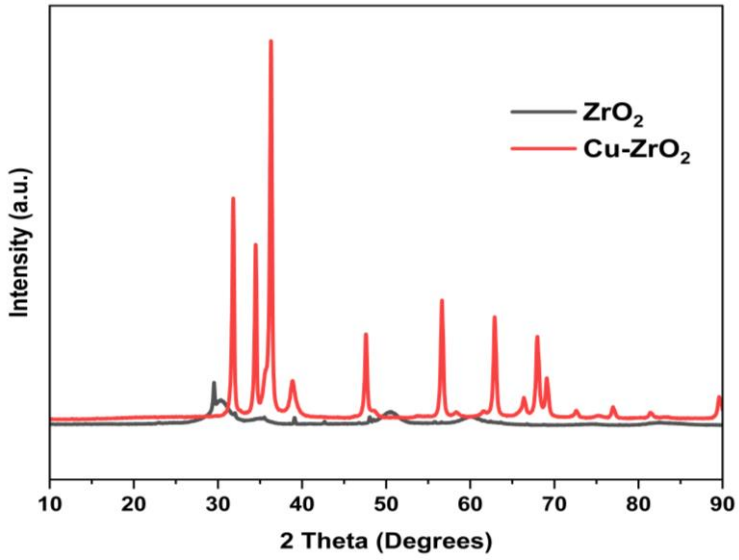

Fig. 1: XRD spectral image of Copper doped Zirconium oxide NPs

It is noted that the synthesized samples are nano regime with spherical shaped particles and in some areas, they are agglomerated due to the synthesis process. The average particle size is calculated using ImageJ software with normal distribution curve fitting and it is found to be 38.3 (Fig. 2d) and 22.1 (Fig. 2b) nm. It was confirmed that from fig. 2 that the Cu^{2+} ions are occupying the interstitial spaces since the orientation of undoped and Cu-doped nanoparticles is different.

During doping, it is impossible to replace Zr^{4+} ions with Cu^{2+} owing to the smallest ionic radius of copper compared to Zr^{4+}, thus it occupies the interstitial lattice sites and produces defects in ZrO_2 and so it decreases the crystallite size from 38.3nm to 22.1nm. There is a strong effect on the morphology and crystallinity of ZrO_2 while doping Cu in ZrO_2. In general, the particle size of the doped metal oxide becomes smaller than the undoped host oxide as consequence of restriction of the motion of crystallites at the interaction on the boundaries between host and dopant crystallites[19].

The chemical composition of the ZrO_2 and Cu doped ZrO_2 nanoparticles was analyzed using EDS as displayed in fig. 3. These analyzed results confirm the presence of zirconium, copper and oxygen from the appearance of Zr, Cu and O peaks. It indicates the purity of the product and without any other signal present in the product.

XPS survey spectrum: The surface composition and elemental oxidation states of the Cu doped ZrO_2 nanoparticles were confirmed using XPS techniques. The XPS spectrum of Cu doped ZrO_2 nanoparticles mainly shows that the composition of Cu, O and Zr species can be observed from the survey and no other elements are detected. The presence of Cu was observed in peaks (Cu $2p_{3/2}$ and $2p_{1/2}$) at 780.3 and 795.8 eV (Fig. 4c), signifying the divalent valence state of copper ions within the ZrO_2 lattice. The high-resolution spectrum of Zr 3d (Fig. 4a) exhibits a prominent peak at a binding energy of 177.8 eV, which corresponds to the Zr $3d_{5/2}$ orbital, confirming the presence of zirconium in an oxidized state, most likely as zirconium dioxide (ZrO_2). The O 1s spectrum (Fig. 4b) displays a strong peak at 529.5 eV, which is attributed to lattice oxygen present within the metal oxide framework, further validating the formation of ZrO_2.

Surface area study: As showed in fig. 5, Brunauer–Emmett–Teller (BET) analysis confirmed that Cu-doped ZrO_2 (Cu-ZrO_2) exhibits enhanced textural properties compared to pure ZrO_2. At a pore volume of 0.0014 cm^3/g, Cu-ZrO_2 showed a higher pore surface area (0.845 units) than ZrO_2 (0.70 units). This trend persisted at lower pore volumes (0.0004 cm^3/g), with Cu-ZrO_2 maintaining a greater surface area (0.50 vs. 0.45 units).

The improvement is attributed to Cu^{2+} doping, which introduces lattice distortions, inhibits particle agglomeration and increases porosity consistent with prior studies on transition metal-doped ZrO_2[22].

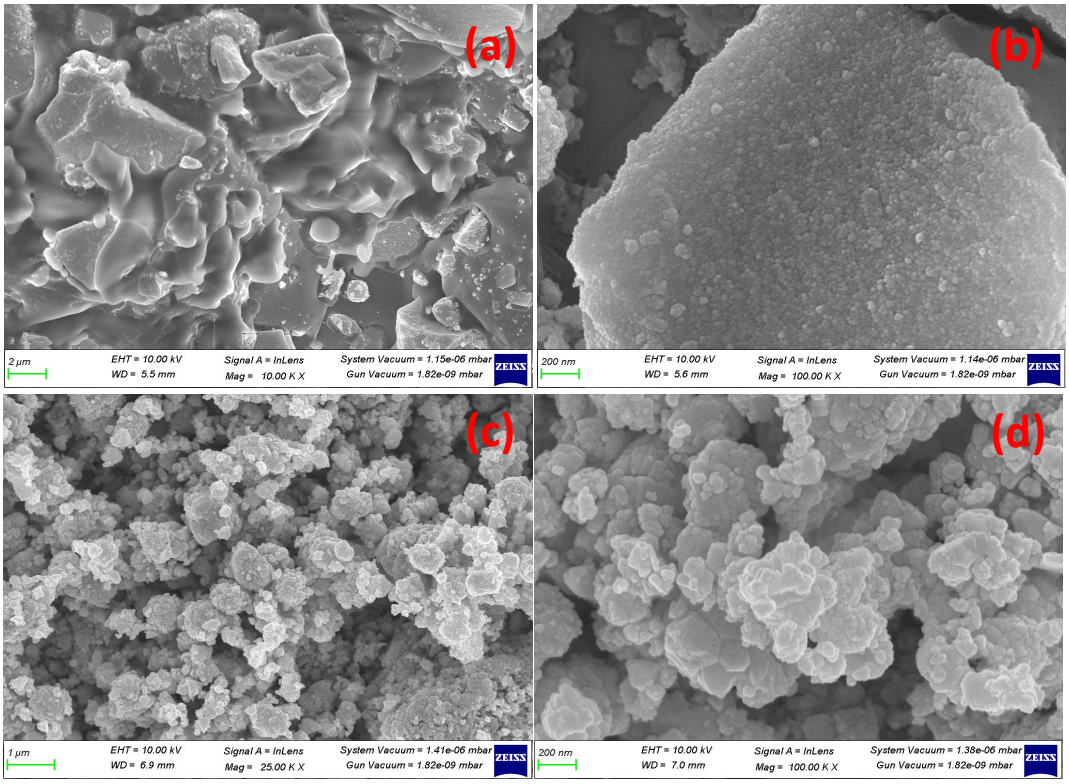

Fig. 2(a-d): SEM micrographs of (a-b) prepared ZrO_2 and (c-d) Cu-doped ZrO_2

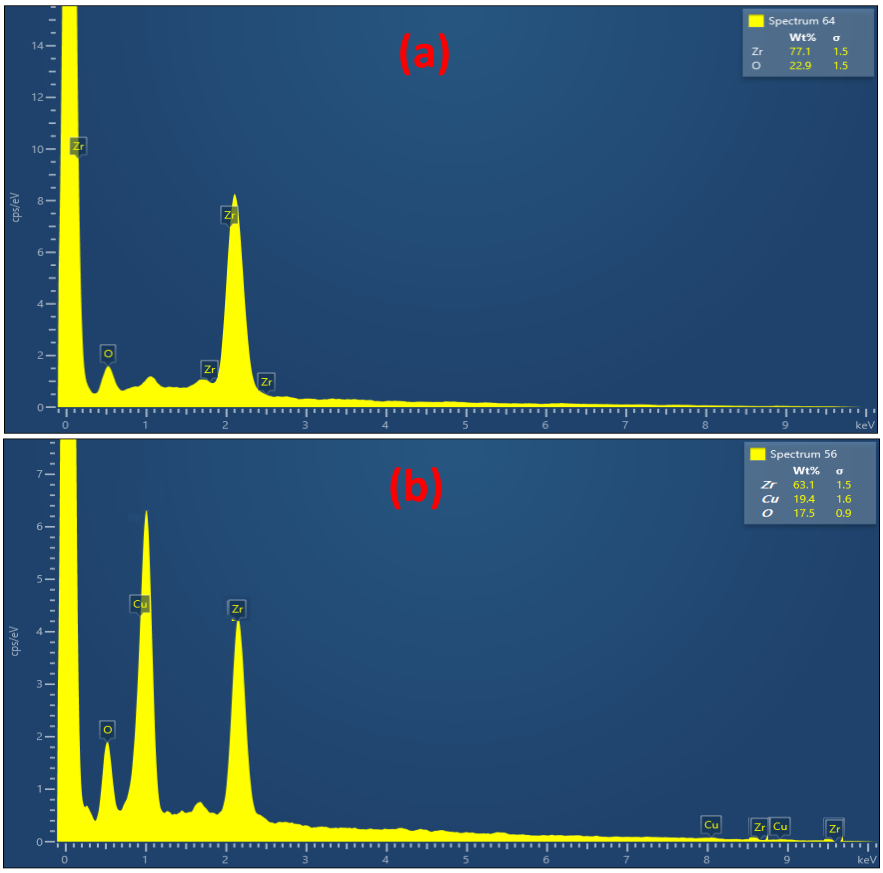

Fig. 3: EDX images of (a) prepared ZrO_2 and (b) Cu-doped ZrO_2

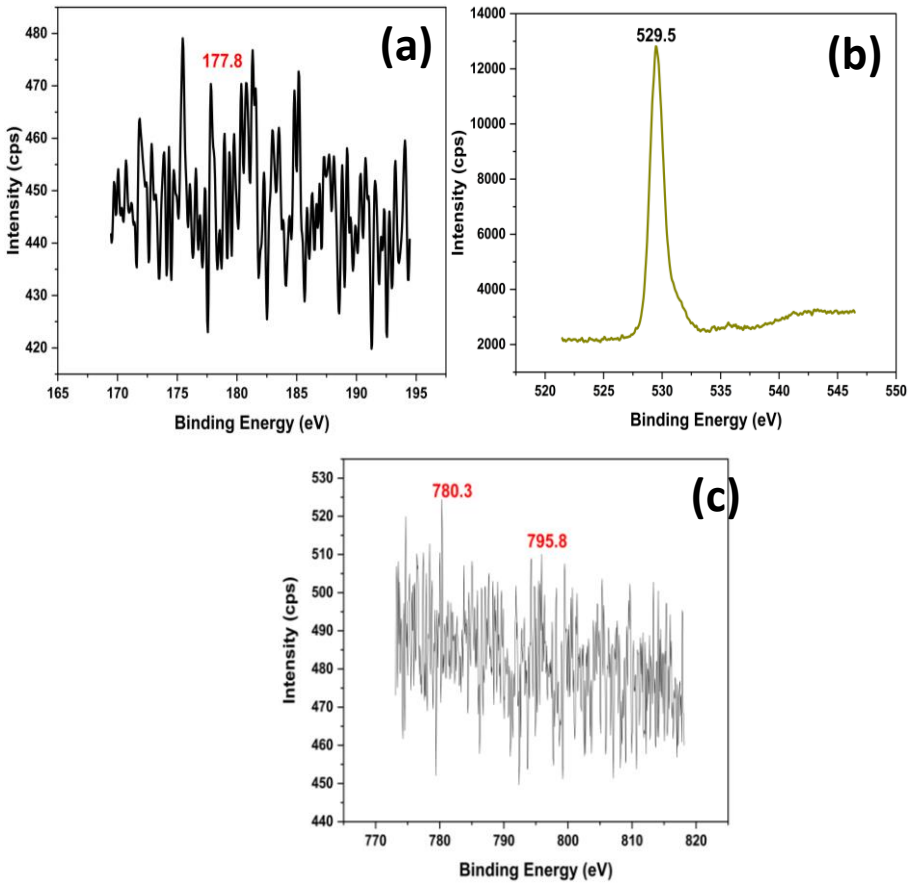

Fig. 4: XPS spectral analysis of prepared Cu-ZrO_2 NPs

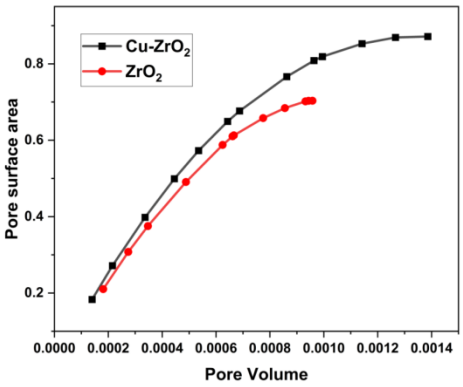

Fig. 5: BET surface area analysis of Cu/ZrO_2 with ZrO_2

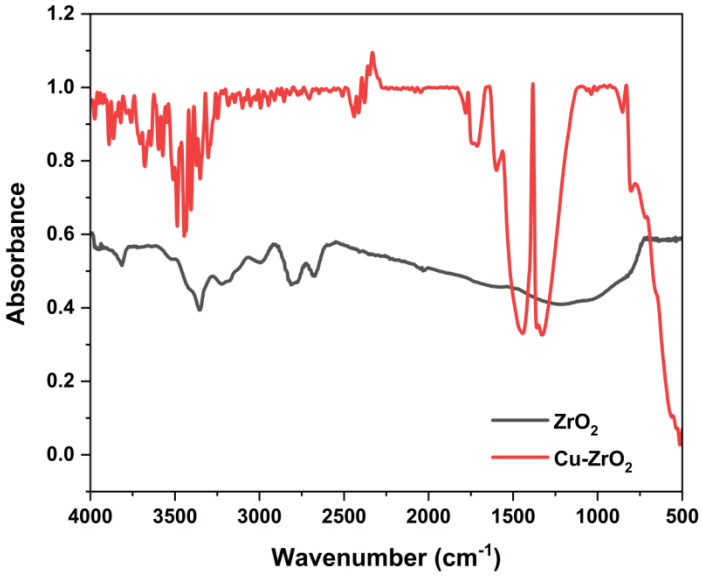

Fig. 6: FTIR spectra of prepared Cu/ZrO_2 and ZrO_2

FTIR spectral analysis: Fourier-transform infrared (FTIR) spectroscopy confirmed the structural characteristics of pristine ZrO_2 and Cu-doped ZrO_2 nanoparticles (Fig. 6). Peaks at 653, 1199, 1493, 2674.9, 2813.7, 3000.8 and 3347.9 cm^{-1} (ZrO_2) and 511, 681, 983, 1325, 1446, 2449 and 3447 cm^{-1} (Cu-ZrO_2) were observed. The broad O-H stretching (3347-3447 cm^{-1}) and bending (1325-1493 cm^{-1}) modes indicate surface hydroxylation [20, 25]. The Zr-O vibrations (511-983 cm^{-1}) confirm the coexistence of tetragonal (511, 653 cm^{-1}) and monoclinic (681, 983 cm^{-1}) phases. A shift toward higher frequencies in Cu-ZrO_2 suggests successful Cu^{2+} incorporation, inducing lattice distortions and oxygen vacancies which enhance surface reactivity.

UV-Vis Spectral analysis: UV-Vis absorption spectra of pure ZrO_2 and Cu doped ZrO_2 NPs are shown in fig. 7. The absorption peak was occurring around 302 nm for the both doped and un-doped samples. The pure ZrO_2 sample shows a sharp decline in absorbance beyond this region, indicating minimal light absorption in the visible range. However, the Cu-doped ZrO_2 sample displays a relatively higher absorbance throughout the UV and near-visible regions compared to pure ZrO_2. This enhancement in optical absorption can be attributed to the incorporation of copper ions into the ZrO_2 lattice, which introduces additional defect states or energy levels within the band structure. Such improved optical properties make Cu-doped ZrO_2 a promising candidate for applications like photocatalysis and dye degradation, where efficient utilization of light energy is essential.

Malachite green (MG) dye degradation: The photocatalytic performance of prepared samples has been tested for degradation of malachite green dye under visible irradiation. Due to the increase in the energy gap of solar light, it is not suitable as a source of photocatalysis, since it is a continuous spectrum. Certain part of spectra is not used for photoelectron hole production. The input energy provided by visible light is large when compared to solar light, thus it is sufficient for band gap excitation of electrons in the photocatalysts[7]. The surface composition of ZrO_2 has a great role in the adsorption of dye to enhance photocatalytic activity[32]. Also, various properties of ZrO_2 polymorphs have a great effect on the adsorption and reaction of dyes.

The optical absorption spectra of the degradation of malachite green (MG) dye using undoped and Cu-doped

ZrO_2 nanoparticles are shown in fig. 8. The strong absorption peak of MG arises at 616nm which is due to the chromophore group. The intensity peak of MG at 616 nm was reduced while increasing the irradiation time. It is because of fragmenting of chromophores in the dye throughout the photocatalytic oxidation The following equation provides the degradation efficiency (E) of MG dye:

$$E = \frac{C0-C}{C0} \times 100\% \quad (3)$$

where 'C_0' is the initial concentration of dye and C is the concentration of MG after visible irradiation. It was observed that Cu-doped ZrO_2 nanoparticles provide faster degradation of MG dye compared to pure ZrO_2. The presence of undoped ZrO_2 nanoparticles degraded the 55% of MG dye in 180 minutes (Fig. 8a) under visible light.

However, copper doped zirconium oxide nanoparticles enhanced the degradation of MG dye from 55% to 96% within 120 minutes (Fig. 8b). This is due to the surface area of the Cu doped ZrO_2 as high due to the low particle size (22.1nm) as compared to ZrO_2. The high surface area provides more active sites for the reaction of photodegradation[32]. Thus copper ions can act as recombination centers and cover the active sites in the host lattice and so enhanced the photocatalytic activity as compared to pure ZrO_2[35]. Due to the morphological change and reduction of crystallite size, doping by Cu ions enhances photocatalytic activity, because Cu-doped ZrO_2 has more oxygen vacancies, it may have higher photocatalytic efficiency[19]. From the outcome of the results, it shows that the copper doped ZrO_2 can effectively enrich the photocatalytic activity.

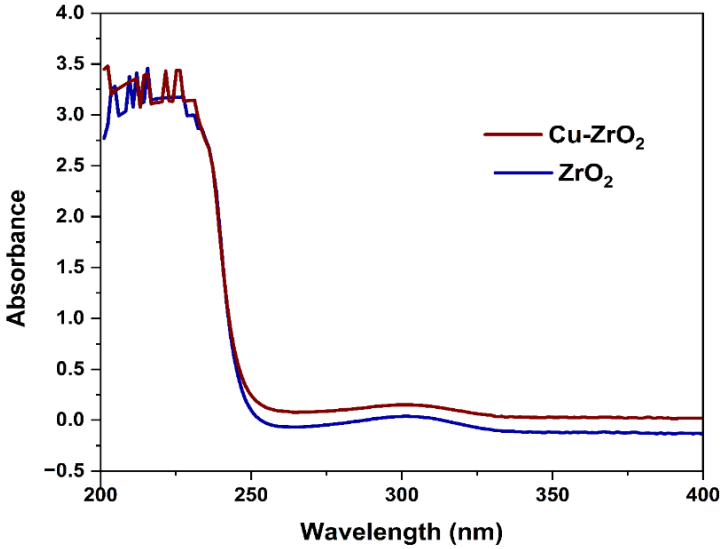

Fig. 7: UV-Vis spectral analysis of prepared samples

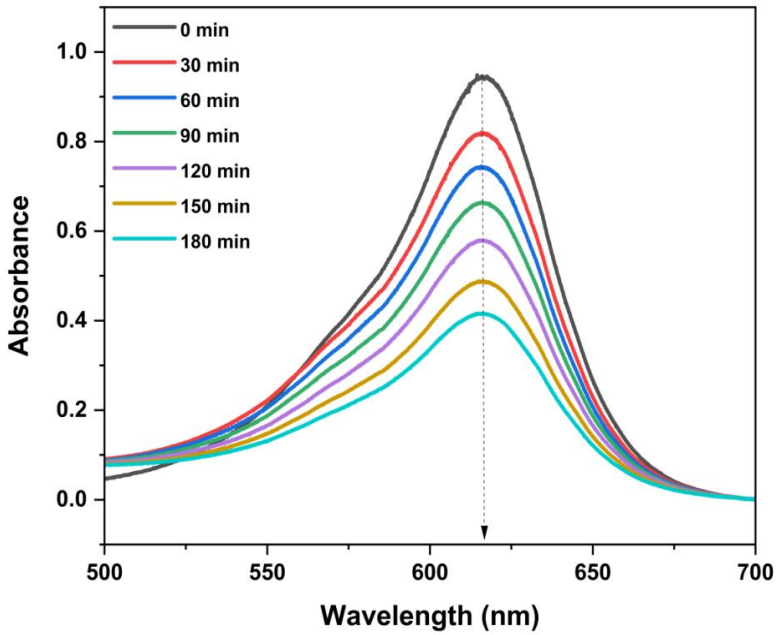

Fig. 8a: MG dye degradation using prepared ZrO_2 NPs

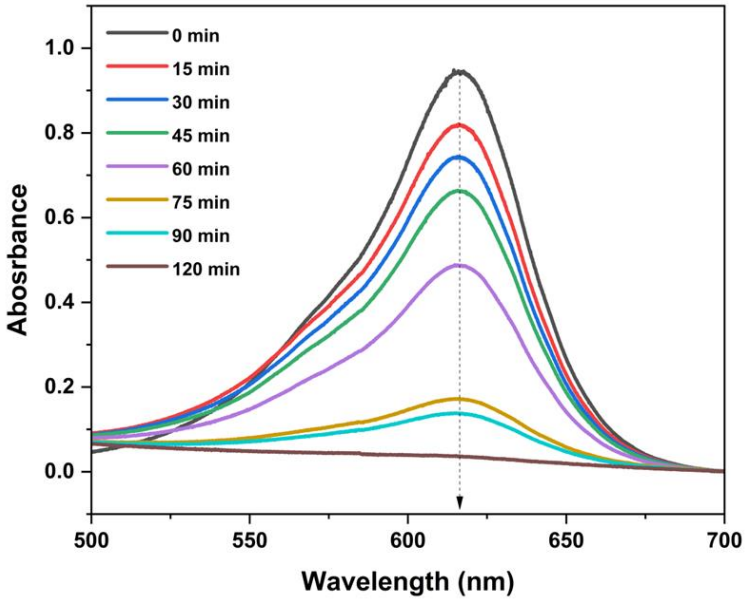

Fig. 8b: MG dye degradation using prepared Cu doped ZrO_2 NPs

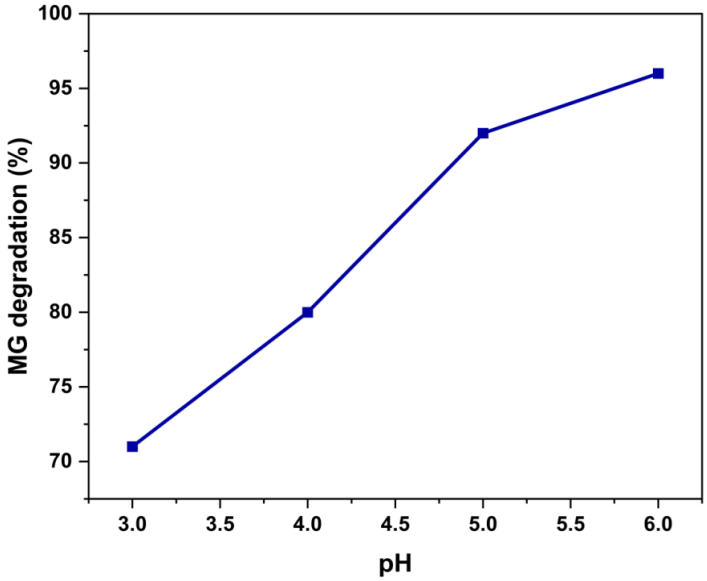

Fig. 9a: Effect of acidic pH on the rate of degradation of MG dye by Cu-ZrO_2 NPs

Optimum conditions for MG degradation

a) Effect of pH: The role of pH in the photodegradation reaction is very prominent as it affects the surface opacity of the adsorbent and the removal of adsorbate from an aqueous solution[23]. The functional groups lie on the surface of the catalyst and dye generates different charges on their respective surfaces through protonation and deprotonation with the concern of pH[11]. Therefore, three different pH (acidic, basic and neutral) were taken in this study to optimize pH for a better photodegradation rate. Based on the results, the maximum degradation rate of MG dye occurred at acidic pH. In order to access the maximum MG dye degradation efficiency at exact acidic pH, we have conducted the experiments at different acidic pH (3, 4, 5 and 6) in this study as shown in fig. 9a. The highest adsorption and 96% destruction of MG occurred at pH 6 in 2h. It was observed that the degradation efficiency of MG dye increased with an increase in solution pH. The probable reason for this behavior may be explained due to the increase of the electrostatic adsorption of cationic MG dye on the Cu doped ZrO_2 catalyst surface dependent on its surface charge[9]. At pH 6, the ZrO_2 surface is negatively charged which increases the electrostatic interaction between the negatively charged copper doped zirconium oxide polymeric and MG cations and leads to strong adsorption with a correspondingly high rate of dye degradation[13].

b) Catalyst loading: On further optimization with catalyst loading from 30 to 60 mg of NPs standard concentration of 10 ppm MG dye and pH 6, the results are presented in fig. 9b. When the catalyst dosage increases, increased amount of photon absorption on the catalyst surface on the nano catalyst surface occurs. The degree of degradation of malachite green dye increased slowly with increasing

catalyst dosage and reached a maximum of about 60 mg. The observed effect can be connected to triggering light penetration into the suspension, which increases deterioration efficiency. Additionally, a more noticeable increase was accomplished with an enhanced reaction time due to the availability of more vacant locations. A similar observation was made by Salarian et al[27].

c) Dye initial concentration: The photocatalytic degradation of MG dye is a complex process that is affected by a number of factors including the pH of solution, catalyst dosage and initial dye concentration. The blanket effect is one of the factors that can affect the rate of degradation. This effect occurs when the dye molecules become so concentrated that they start to cover the active sites on NPs surface. The optimum initial MG dye concentration for the degradation of MG dye was 10 mg/L. At this concentration, the blanket effect was pronounced very low and the degradation rate was reduced. From the fig. 9c, it was observed that the degradation efficiency decreases with an increase in the initial concentration of MG dye. At a lower concentration of 5 mg/L, nearly 100% degradation of the dye is achieved, indicating the high photocatalytic activity of Cu-ZrO_2 under these conditions.

As the dye concentration increases to 10 mg/L and 15 mg/L, the degradation efficiency gradually decreases to approximately 96% and 92% respectively. A significant decline in degradation efficiency is observed at 20 mg/L where only around 80% degradation is achieved. However, if the dye concentration is too high, the blanket effect will become more pronounced and the degradation rate will decrease. This trend can be attributed to the saturation of available active sites on the Cu-ZrO_2 surface at higher dye concentrations.

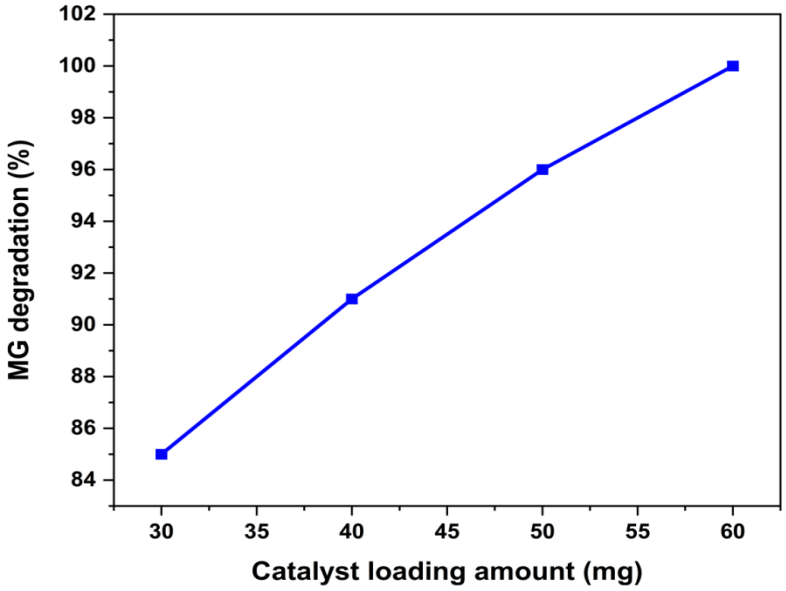

Fig. 9b: Effect of catalyst dose (30-60mg) on the rate of degradation of MG dye by Cu-ZrO_2 nanocatalyst

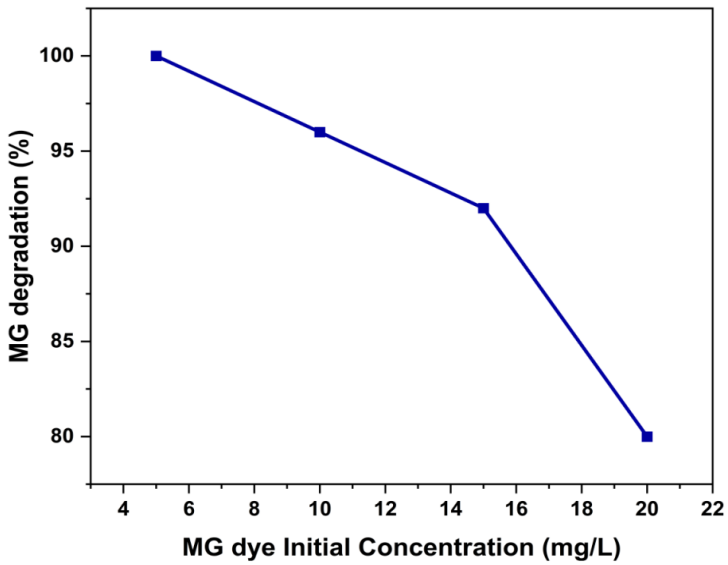

Fig. 9c: Effect of MG dye Initial Concentration (4-20 mg/L) on degradation of MG dye by Cu-ZrO_2 nanocatalyst

At lower concentrations, sufficient active sites and light penetration are available to effectively degrade the dye molecules. However, as the concentration increases, the excess dye molecules compete for the limited active sites, leading to reduced degradation efficiency. Additionally, higher dye concentrations can hinder light penetration, limiting the generation of reactive species required for the photocatalytic degradation process.

Possible mechanism: A feasible charge carrier transfer mechanism for Cu-improved ZrO_2's photoactivity is shown in figure 10. Using visible light to photoexcite ZrO_2, electron-hole (e-/h+) pairs are generated. The recombination of the e-/h+ pairs in alone was trapped and suppressed by the formation of impurity levels in the band gap of ZrO_2 as a result of the addition of Cu[4]. In addition to participating in photodegradation or antibacterial activity, the generated reactive oxygen species such as hydroxyl, peroxyl radicals and holes (h^+) can also speed up some reduction processes. The surface hydroxyl ion may interact with the h^+ in valence band (VB) and H_2O to produce extremely reactive hydroxyl radicals as shown in equations 4 to 11.

$$Cu/ZrO_2 + light \rightarrow Cu/ZrO_2\ (h^+) + Cu/ZrO_2\ (e^-) \quad (4)$$
$$Cu/ZrO_2(_{VB}h^+) + H_2O \rightarrow Cu/ZrO_2 + OH^- + H^+ \quad (5)$$
$$Cu/ZrO_2(_{VB}h^+) + OH^- \rightarrow Cu/ZrO_2 + {}^{\cdot}OH \quad (6)$$
$$Cu/ZrO_2(_{CB}e^-) + O_2 \rightarrow Cu/ZrO_2 + {}^{\cdot}O_2^- \quad (7)$$
$$Cu/ZrO_2(_{CB}e^-) + {}^{\cdot}O_2^- + H_2O \rightarrow Cu/ZrO_2 + HO_2{}^{\cdot} + OH^- \quad (8)$$
$$Cu/ZrO_2(_{CB}e^-) + HO_2{}^{\cdot} + H^+ \rightarrow Cu/ZrO_2 + H_2O_2 \quad (9)$$
$$Cu/ZrO_2(_{CB}e^-) + H_2O_2 \rightarrow Cu/ZrO_2 + OH^{\cdot} + OH^- \quad (10)$$
$$^{\bullet}OH + {}^{\bullet}O_2^- + MG \rightarrow \text{Degradation products} \quad (11)$$

Stability and reusability: The photocatalyst was further examined for the recyclability and sustainability over the malachite green dye under visible light irradiations. In that concern, the photocatalyst was collected during the degradation process and washed thoroughly with water followed by ethanol. Fig. 11a illustrates the reusability performance of the Cu-doped zirconium oxide (Cu-ZrO_2) photocatalyst for the degradation of Malachite Green (MG) dye over six consecutive cycles.The degradation efficiency is seen to decrease gradually with each reuse cycle. During the first run, the catalyst exhibited nearly 100% degradation efficiency, indicating excellent photocatalytic activity.

However, with subsequent cycles, a slight reduction in efficiency is observed. In the second and third runs, the degradation efficiency remains above 95%, demonstrating good catalyst stability. From the fourth run onwards, a noticeable decline is evident, with degradation dropping to around 90% in the fourth run and approximately 87% in the fifth run. By the sixth run, the degradation efficiency decreases further to nearly 82%. The recycle experiment was carried out for successive six runs to find out the 18% loss in six runs (Fig. 11a) due to the loss of photocatalyst during the washing process. Interestingly, the photocatalyst has the crystalline structure though five cycles were completed as shown in fig. 11b concluding that this Cu-ZrO_2 NPs can be reused and is stable for large scale photocatalytic degradation of MG dye.

Various catalysts have been synthesized to enhance the efficiency of photocatalysis. Among these, metal-oxide nanoparticles stand out owing to their low toxicity and ease of transformation to hydroxides or oxides. An important attribute is the material's bandgap, which determines the energy difference between the oxidation and reduction processes.

The bandgap significantly influences the photocatalytic performance of nanomaterials where a narrower bandgap corresponds to higher photocatalytic activity. An increase in light absorption accompanied by a red shift indicates that the photocatalyst maintains its performance over time, making it both reliable and cost-effective[30].

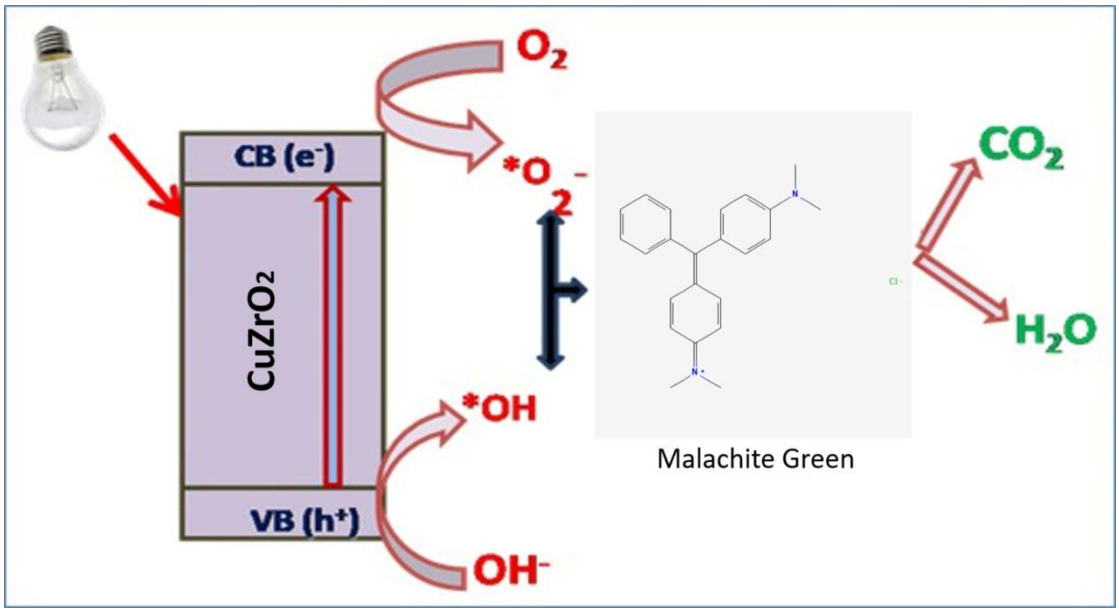

Fig. 10: Schematic representation of possible mechanism of photodegradation

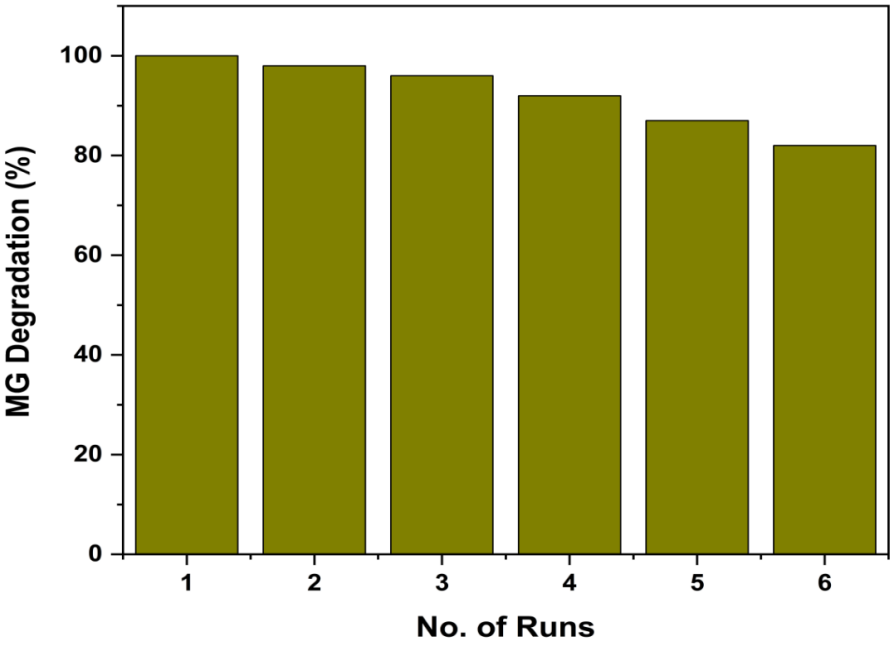

Fig. 11a: Reusability of tested Cu doped ZrO_2 NPs

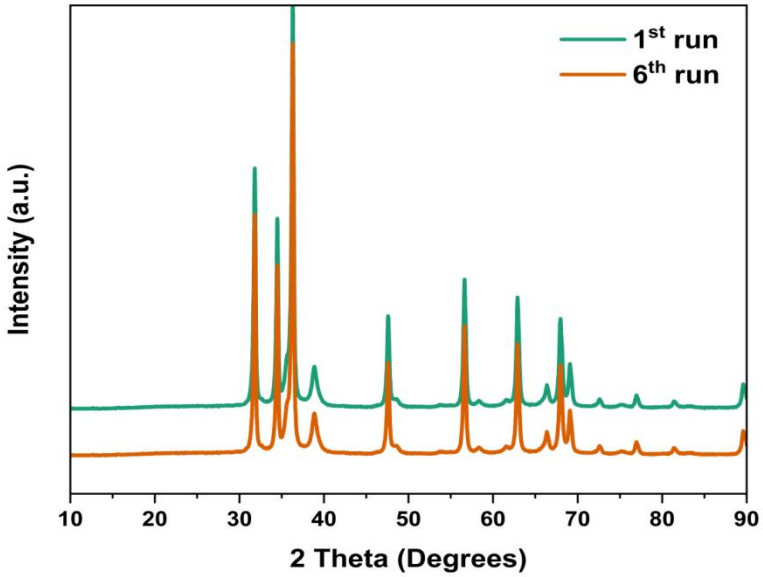

Fig. 11b: Sustainability of recycled Cu doped ZrO_2 NPs

Photocatalysts are commonly produced using nanoparticles of metal oxides such as TiO_2, ZnO, Bi_2O_3, Fe_2O_4, WO_3, CuO, Cu_2O and SnO_2[21]. These metal-oxide nanoparticles come in various shapes including nanoparticles, nanospheres, nanofibers, nanotubes, nanoribbons and nanosheets. In table 1, a comparison has been provided for the degradation of MG dye in previous studies using different metal-oxide nanoparticles, along with the experimental conditions employed.

Antimicrobial activity: The antibacterial activity of Cu-ZrO_2 and pure ZrO_2 NPs was systematically evaluated against both *Staphylococcus aureus* (Gram-positive) and *Escherichia coli* (Gram-negative) using the agar well diffusion method at concentrations of 500 µg/mL, 200 µg/mL and 100 µg/mL. Pure ZrO_2 exhibits a larger zone of inhibition around 8mm against Gram-positive pathogen namely *Staphylococcus aureus* compared to other bacteria. Cu doped ZrO_2 nanoparticles exhibit a higher zone of inhibition against both Gram-positive and negative bacteria. The measured values of the inhibition zone in terms of mm are presented in tables (2, 3). Fig. 12 clearly shows that the synthesized Cu-doped ZrO_2 samples have more activity against *Escherichia coli*. The copper doping enhances the antibacterial properties, likely due to the synergistic effect of copper ions which disrupt bacterial cell membranes, generate reactive oxygen species and interfere with essential cellular processes[35].

Conclusion

ZrO_2 and Cu-ZrO_2 nanoparticles were successfully synthesized using a simple and cost-effective sol-gel

combustion method. The structural, morphological and optical studies confirmed that the incorporation of copper ions into the ZrO_2 lattice reduced the crystallite size, increased surface area and enhanced light absorption in the visible region.

The Cu-ZrO_2 nanoparticles exhibited superior photocatalytic activity by achieving 96% degradation of toxic Malachite Green dye under visible light within 120 minutes, which is significantly higher than pure ZrO_2. The photocatalytic efficiency was strongly influenced by factors such as pH, catalyst dosage and dye concentration, with optimal degradation observed at pH 6 and 10 mg/L dye concentration.

Table 1
Some previous studies conducted for malachite green dye degradation by various metal-oxide-based nanoparticles[33].

Metal Oxide	Synthesis Technique	Morphology	Photocatalytic Experimental Setup	Degradation Efficiency [%]
Xanthan gum/SiO_2	Ultra-sonication with polymerization	Lobule	10 mg catalyst, 450 ppm of MG dye, pH = 7, the temperature of 30 °C, 480 min	99.5
$CuMn_2O_4$	Co-precipitation method	Flake-like structure	Daylight, 60 min. UV light, 60 min, bandgap value 2.54 eV	94.80,
Chitosan/TiO_2	–	Spherical nanoparticles	70 ppm, 90 min, bandgap value ≈ 3 eV	90.70
rGO/CuS	Co-precipitation method	Irregular hexagonal	100 mg photocatalyst, 10 ppm dye,under sunlight at room temperature, bandgap value 2 eV	97.60
nFe_2O_4	Probe sonication	Spongy like	Under sunlight, UV lamp, it took about 180 min, 2.4 eV	98–88
Hematite	Combustion	Spherical and irregular structure	Presence of H_2O_2, 20 ppm dye, UV source of 250 W, 0.1 g catalyst, 70 min, bandgap 1.45 eV	100
Cu_2O	Sonochemical method	Uniform Icosahedron	10 ppm dye, 10 mg catalyst, visible lamp, 45 min, 2.26 eV	91.89
ZnO	Sol–gel method	Spherical structure	10 ppm dye concentration, 20 mg catalyst, UV lamp, 40 min, bandgap 3.3 eV	99
CeO_2	Chemical precipitation method	Cubic fluorite	Visible light, 80 min, bandgap value 2.90 eV	99
TiO_2	Micro-emulsion method	Spherical	10 mg catalyst, 10 ppm dye, visible light, 50 min, bandgap 3.2 eV	96.40
ZnO/CuO	Hydrothermal method	–	0.2 g catalyst, 15 ppm dye, pH-10, UV lamp, 240 min, bandgap value 4.42 eV	82
ZnO:Ag	Soft chemical method	Spherical structure	45 min, 500-Watt tungsten lamp, 60 min, visible light, pH 4.66, temperature of 30 °C, bandgap of 2.67 eV	88.8
$CuWO_4$-RGO	Hydrothermal method	Agglomerated with polycrystalline nature	2 ppm dye, 50 mg catalyst, 370 W mercury halide visible light, 60 min, 2.2 eV	93
$CuWO_4$-GO	Ball-milling method	Microstructure	0.05 g catalyst, 10 ppm dye, visible lamp, 80 min,	95
Fe-Cu binary oxides	Electron spun method	Hair like structure	3 mg catalyst, 100 ppm dye solution, pH = 1, UV lamp, 60 min	91.40
Ag-Mn- oxide nanoparticles	Wet chemical precipitation method		aqueous solution containing 25 ppm of MG, 100 min 60 min of degradation, at pH 4, 7 and 10	92%
Cu-ZrO_2	Combustion mediated Sol-gel synthesis	Spherical Shape	Aqueous solution containing 10 ppm of MG, 120min of degradation, at pH - 7	96% (In this study)

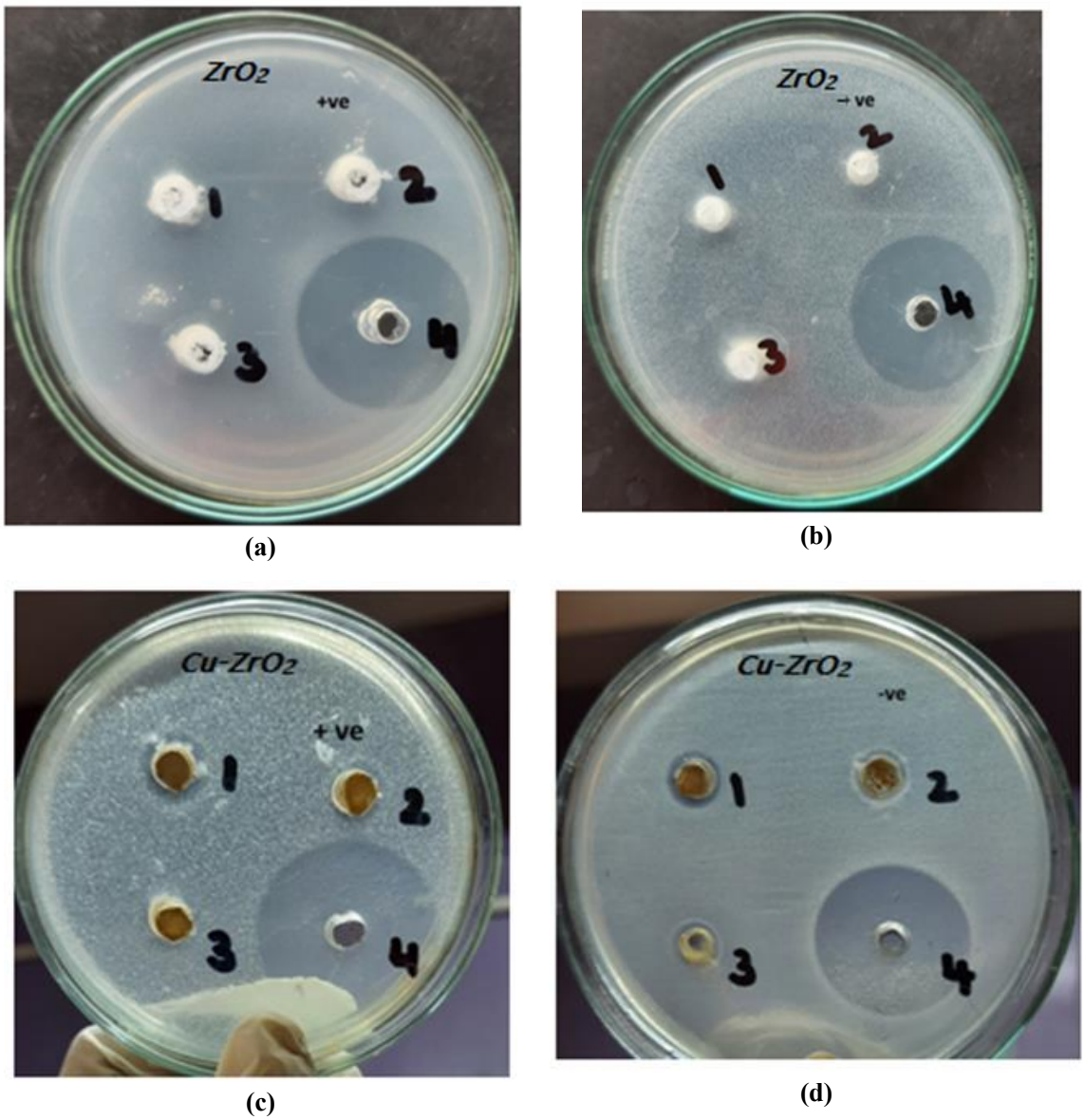

Fig. 12: Antibacterial property of ZrO_2 against (a) *S.aureus* (b) *E.coli* and Cu-ZrO_2 against (c) *S.aureus* (d) *E.coli*

Table 2
Antibacterial activity showing the diameter of the zones on organism of bacteria i.e. Gram-negative (*E.coli*)

Test Compound	Zone of Inhibition (mm)			
	500 µg/mL	200 µg/mL	100 µg/mL	Control
Cu-ZrO_2	10	8	6	14
ZrO_2	8	8	6	13

Table 3
Antibacterial activity showing the diameter of the zones on organism of bacteria i.e. Gram-positive (*S.aureus*)

Test Compound	Zone of Inhibition (mm)			
	500 µg/mL	200 µg/mL	100 µg/mL	Control
Cu-ZrO_2	8	6	4	16
ZrO_2	6	5	4	16

Furthermore, Cu-ZrO_2 nanoparticles demonstrated enhanced antibacterial activity against both Gram-positive (*Staphylococcus aureus*) and Gram-negative (*Escherichia coli*) bacteria compared to undoped ZrO_2. The improved performance is attributed to the synergistic effect of copper doping which increased oxygen vacancies, created structural defects and enhanced the generation of reactive oxygen species. The Cu-ZrO_2 photocatalyst also displayed good stability and reusability over multiple cycles, confirming its potential for practical environmental applications. Overall,

the results suggest that Cu-doped ZrO_2 nanoparticles are promising multifunctional materials for wastewater treatment and antibacterial applications due to their excellent photocatalytic efficiency, antibacterial properties and structural stability.

References

1. Adinarayana D., Annapurna N., Mohan B.S. and Douglas P., Enhanced photocatalytic removal of Cr (VI) and Rhodamine B from water using plant-mediated CdS nanoparticles: Mechanistic insights and environmental applications, *Desalination and Water Treatment*, **320**, 100593 **(2024)**

2. Anku W.W., Oppong S.O.B., Shukla S.K., Agorku E.S. and Govender P.P., Cobalt doped ZrO_2 decorated multiwalled carbon nanotube: A promising nanocatalyst for photodegradation of indigo carmine and eosin Y dyes, *Progress in Natural Science: Materials International*, **26(4)**, 354-361 **(2016)**

3. Arjun A. et al, Study of Copper Doped Zirconium Dioxide Nanoparticles Synthesized via Sol–Gel Technique for Photocatalytic Applications, *J. Inorg. Organomet. Polym.*, **30**, 4989–4998 **(2020)**

4. Arredonoda E.J.L., Maldonado A., Asomoza R., Acosta D.R., lira M.A.M. and Olvera M.L., Indium-doped ZnO thin films deposited by the sol–gel technique, *Thin Solid Films*, **490(2)**, 132–136 **(2005)**

5. Atari D.O. and Luginaah I.N., Assessing the distribution of volatile organic compounds using land use regression in Sarnia, "Chemical Valley," Ontario, Canada, *Environmental Health*, **8**, 1-14 **(2009)**

6. Botsa S.M. and Basavaiah K., Fabrication of multifunctional TANI/Cu2O/Ag nanocomposite for environmental abatement, *Scientific Reports*, **10(1)**, 14080 **(2020)**

7. Botsa S.M., Seetharam P., Manga Raju I., Suresh P., Satyanarayana G., Sambasivam S., Uppugalla S. and Tejeswararao D., Nanohybrid material of Co–TiO2 and optical performance on methylene blue dye under visible light illumination, *Hybrid Advances*, **1**, 10008 **(2022)**

8. Chowdhary P., Bharagava R.N., Mishra S. and Khan N., Role of Industries in Water Scarcity and its Adverse Effects on Environment and Human Health, Environmental Concerns and Sustainable Development, 235-256 **(2020)**

9. Diab K.E., Salama E., Hassan H.S., El-Moneim A.A. and Elkady M.F., Biocompatible MIP-202 Zr-MOF tunable sorbent for cost-effective decontamination of anionic and cationic pollutants from waste solutions, *Scientific Reports*, **11**, 1–13 **(2021)**

10. Elkady M., Hassan H.S. and Hashim A., Immobilization of Magnetic Nanoparticles onto Amine-Modified Nano-Silica Gel for Copper Ions Remediation, *Materials*, **9**, 460 **(2016)**

11. Farrokhi M., Hosseini S., Yang J. and Siboni M., *Water, Air & Soil Pollution*, **225**, 2113 **(2014)**

12. Gopal R. et al, Versatile fabrication and characterization of Cu-doped ZrO_2 nanoparticles: enhanced photocatalytic and photoluminescence properties, *J. Mater. Sci.: Mater. Electron.*, **31**, 7232–7246 **(2020)**

13. Gar Alalm M., Samy M., Ookawara S. and Ohno T., Immobilization of S-TiO_2 on reusable aluminum plates by polysiloxane for photocatalytic degradation of 2,4-dichlorophenol in water, *J. Water Process Eng.*, **26**, 329–335 **(2018)**

14. Hammad A., Haitham M., El-Bery H.M., EL-Shazly A.H. and Elkady M., Effect of WO3 Morphological Structure on its Photoelectrochemical Properties, *Int. J. Electrochem. Sci.*, **13**, 362–372 **(2018)**

15. Hammad A., Akihiko A., Xing Z., Akira Y., Daiki O., Teppei Y., EL-Shazly A., Elkady M. and Hisao Y., Photodeposition conditions of silver cocatalyst on titanium oxide hotocatalyst directing product selectivity in photocatalytic reduction of carbon dioxide with water, *Catal. Lett.*, **150**, 1081–1088 **(2020)**

16. Hong N.H., Kanoun M.B., Goumri-Said S., Song J.H., Chikoidze E., Dumont Y. and Kurisu M., The origin of magnetism in transition metal-doped ZrO2 thin films: experiment and theory, *J. Phys. Condens. Matter*, **25**, 436003 **(2013)**

17. Hyun-Sig K.I.L., Su-Hyun H.W.A.G., Je-Hyeok R.Y.U., Dae-Young L.I.M. and Seung-Beom C.H.O., Glycothermal synthesis of nanocrystalline ZrO2 powders at low temperature without mineralizers, *J. Ceram. Soc. Japan*, **120(1398)**, 52-57 **(2012)**

18. Jeba R., Radhika S., Padma C.M. and Ascar Davix X., Structural, Optical, Thermal, Magnetic Properties of Zirconia Nanorods and their Photocatalytic and Antimicrobial Properties, *J. Water Environ. Nanotechnol.*, **6(3)**, 252-264 **(2021)**

19. Jeba R., Radhika S., Padma C.M. and AscarDavix X., The influence of Cu doped ZrO2 catalyst for the modification of the rate of a photoreaction and forming microorganism resistance, *J. Water Environ. Nanotechnol.*, **7(4)**, 351-362 **(2022)**

20. Keiteb A.S., Saion E., Zakaria A. and Soltani N., Structural and Optical Properties of Zirconia Nanoparticles by Thermal Treatment Synthesis, *J. Nanomaterials*, **2016**, 1913609 **(2016)**

21. Krishna Kumar A.S., Warchol J., Matusik J., Tseng W.L., Rajesh N. and Bajda T., Heavy metal and organic dye removal via a hybrid porous hexagonal boron nitride-based magnetic aerogel, *NPJ Clean Water*, **5**, 24 **(2022)**

22. Kumar J.S., Shyamala P., Gouthamsri S. and Ramanaiah M., Efficient Removal of Methylene Blue and Inactivation of Pathogens by Cobalt Doped ZrO2 Nanoparticles, *ECS J. Solid State Sci. Technol.*, **14**, 053009 **(2025)**

23. Melissa Talbi, Ahmed Adjebli, Karim Tighilet, Mustapha Louardiane and Abdelaziz Messis, Time series forecasting cancers cases in Algeria using double exponential smoothing method, *Res. J. Biotech.*, **19(3)**, 1–12 **(2024)**

24. Perez C., Pauli M. and Bazerque P., An Antibiotic Assay by Agar Well Diffusion Method, *Acta Biologiae et Medicinae Experimentalis*, **15**, 113-115 **(1990)**

25. Qu X., Song H., Pan G., Bai X., Dong B., Zhao H., Dai Q., Zhang H., Qin R. and Lu S., Three-Dimensionally Ordered

Macroporous ZrO_2:Eu^{3+}: Photonic Band Effect and Local Environments, *J. Phys. Chem. C*, **113**, 5906-5911 **(2009)**

26. Rani R., Reddy U., Sharma P., Mukherjee P., Mishra A., Kuila A., Sim L.C. and Saravanan P., A review on the progress of nanostructure materials for energy harnessing and environmental remediation, *Journal of Nanostructure in Chemistry*, **8**, 255–291 **(2018)**

27. Salarian A.A., Hami Z., Mirzaei N., Mohseni S.M., Asadi A., Bahrami H., Vosoughi M., Alinejad A. and Zare M.R., N-doped TiO_2 nanosheets for photocatalytic degradation and mineralization of diazinon under simulated solar irradiation: Optimization and modeling using a response surface methodology, *Journal of Molecular Liquids*, **220**, 183–191 **(2016)**

28. Sharma S. and Kaur A., Various methods for removal of dyes from industrial effluents: A review, *Indian J. Sci. Technol.*, **11**, 1–21 **(2018)**

29. Sree G.S., Ranjitha K.V.B., Reddy B.J.M., Mohan B.S. and Kant C.R., Fabrication of RGO based bimetal oxides ternary composite for deterioration of handloom dye and pathogens from polluted water, *Inorganic Chemistry Communications*, **155**, 111054 **(2023)**

30. Sundar K.P. and Kanmani S., Progression of Photocatalytic reactors and its comparison: A Review, *Chemical Engineering Research and Design*, **154**, 135 **(2020)**

31. Tijani J.O., Ugochukwu O., Fadipe L., Bankole M., Abdulkareem A. and Roos W., Photocatalytic degradation of local dyeing wastewater by iodine-phosphorus co-doped tungsten trioxide nanocomposites under natural sunlight irradiation, *J. Environ. Manage.*, **236**, 519-533 **(2019)**

32. Tsoncheva T., Genova I., Dimitrov M., Sarcadi-Priboczki E., Venezia A.M., Kovacheva D., Scotti N. and dal Santo V., Nanostructured copper-zirconia composites as catalysts for methanol decomposition, *Applied Catalysis B: Environment and Energy.*, **165**, 599-610 **(2015)**

33. Xu Z. et al, Enhanced Photocatalytic Degradation of Malachite Green Dye Using Silver–Manganese Oxide Nanoparticles, *Molecules*, **28**, 6241 **(2023)**

34. Yusuff A.S., Olateju I.I. and Adesina O.A., TiO_2/anthill clay as a heterogeneous catalyst for solar photocatalytic degradation of textile wastewater: Catalyst characterization and optimization studies, *Materialia*, **8**, 100484 **(2019)**

35. Zhuang H., Bai S., Lio X. and Yan Z., Structure and performance of Cu/ZrO2 catalyst for the synthesis of methanol from CO2 hydrogenation, *Journal of Fuel Chemistry and Technology*, **38**, 462–467 **(2010)**.

(Received 10th July 2025, accepted 14th August 2025)